




# ELAVL2-directed RNA regulatory network drives the formation of quiescent primordial follicles

Yuzuru Kato<sup>1,2,\*</sup> , Tokuko Iwamori<sup>3</sup>, Youichirou Ninomiya<sup>1,†</sup>, Takashi Kohda<sup>4</sup> , Jyunko Miyashita<sup>1</sup>, Mikiko Sato<sup>1</sup> & Yumiko Saga<sup>1,2,\*\*</sup> 

## Abstract

Formation of primordial follicles is a fundamental, early process in mammalian oogenesis. However, little is known about the underlying mechanisms. We herein report that the RNA-binding proteins ELAVL2 and DDX6 are indispensable for the formation of quiescent primordial follicles in mouse ovaries. We show that *Elavl2* knockout females are infertile due to defective primordial follicle formation. ELAVL2 associates with mRNAs encoding components of P-bodies (cytoplasmic RNP granules involved in the decay and storage of RNA) and directs the assembly of P-body-like granules by promoting the translation of DDX6 in oocytes prior to the formation of primordial follicles. Deletion of *Ddx6* disturbs the assembly of P-body-like granules and severely impairs the formation of primordial follicles, indicating the potential importance of P-body-like granules in the formation of primordial follicles. Furthermore, *Ddx6*-deficient oocytes are abnormally enlarged due to misregulated PI3K-AKT signaling. Our data reveal that an ELAVL2-directed post-transcriptional network is essential for the formation of quiescent primordial follicles.

**Keywords** DDX6; ELAVL2; P-body-like granules; post-transcriptional gene regulation; primordial follicles

**Subject Categories** Development; RNA Biology

**DOI** 10.15252/embr.201948251 | Received 8 April 2019 | Revised 28 September 2019 | Accepted 4 October 2019 | Published online 28 October 2019

**EMBO Reports (2019) 20: e48251**

## Introduction

Long-term reproduction of mammalian females is achieved by controlled sustainability and growth of the most primitive ovarian follicles called primordial follicles, which are composed of a single oocyte and a few of the supporting somatic cells, granulosa cells. Given the importance of primordial follicles as a finite reservoir of eggs in mammalian ovaries, understanding the molecular

mechanisms underlying the formation and sustainability of primordial follicles is essential for reproductive biology and medicine.

Mammalian oogenesis begins once primordial germ cells enter the embryonic ovary, where female gonocytes (or oogonia) proliferate with incomplete cytokinesis. Therefore, cells are connected to each other via intercellular bridges [1]. Eventually, gonocytes initiate meiosis after receiving retinoic acid signaling [2,3]. Primordial follicles arise from oocytes in cysts by breaking down intercellular connections between oocytes, a process termed cyst breakdown, which occurs within a few days after birth in mice [4]. Substantial effort has been made to understand the molecular mechanisms underlying the formation of primordial follicles. FIGLA was initially identified as an oocyte-specific transcription factor required for primordial follicle formation [5]. Subsequently, several signaling pathways, Notch, TGF $\beta$ , and JNK, were reported to be involved in this process [6–9]. More recently, *in vitro* production of functional eggs from primordial germ cells and pluripotent stem cells has been achieved in mice, which provides a great opportunity to understand the molecular basis of primordial follicle formation [10,11]. However, the production of quiescent primordial follicles remains challenging because follicle growth is simultaneously activated *in vitro*. In other words, these studies raised a new question of how primordial follicles become quiescent.

In addition to transcriptional gene regulation, post-transcriptional RNA regulation also plays a fundamental role in the regulation of gene expression. Traditionally, studies on reproductive biology have documented integral contributions of post-transcriptional RNA regulation mediated by species-specific and evolutionarily conserved RNA-binding proteins (RBPs) to oocyte development [12]. Consistent with this, many important processes of mammalian oogenesis, including sexual differentiation and meiosis in embryonic ovaries, and oocyte growth or maturation in postnatal ovaries, require the functions of RBPs [13–18]. However, the role of post-transcriptional RNA regulation in primordial follicle formation remains unknown. In this regard, several studies have suggested some mechanistic differences in terms of post-transcriptional RNA regulation between oocytes in cysts and primordial follicles. The expression of MSY2, a

1 Division of Mammalian Development, Genetic Strains Research Center, National Institute of Genetics, Mishima, Shizuoka, Japan

2 Department of Genetics, SOKENDAI, Mishima, Shizuoka, Japan

3 Department of Biomedicine, Research Center for Human Disease Modeling, Graduate School of Medical Sciences, Kyushu University, Fukuoka, Japan

4 Faculty of Life and Environmental Sciences, University of Yamanashi, Kofu, Yamanashi, Japan

\*Corresponding author. Tel: +81 55 981 6832; Fax: +81 55 981 6828; E-mail: yukato@nig.ac.jp

\*\*Corresponding author. Tel: +81 55 981 6829; Fax: +81 55 981 6828; E-mail: ysaga@nig.ac.jp

†Present address: Research Centre for Medical Bigdata, National Institute of Informatics, Tokyo, Japan

germline-specific RBP involved in messenger RNA (mRNA) stability and translational suppression, was reported to precede primordial follicle formation [5,15,19,20]. In addition, another germline-specific RBP, DAZL, is translationally suppressed coinciding with the formation of primordial follicles [21]. These observations prompted us to investigate the roles of post-transcriptional RNA regulation in the formation of primordial follicles.

In this study, we explored RBPs involved in the formation of primordial follicles in the mouse and identified ELAVL2 (embryonic lethal and abnormal vision-like 2) as an essential RBP. ELAVL2 (also known as HuB) is a member of the ELAVL RNA-binding proteins, which promote translation by associating with mRNAs containing AU-rich elements [22–24]. We found that ELAVL2 associates with mRNAs encoding components of stress granules and processing bodies (P-bodies), cytoplasmic ribonucleoprotein (RNP) granules involved in mRNA decay, storage, or translational stalling [25], in the ovary. Indeed, we discovered that large P-body-like granules were assembled in oocytes prior to the formation of primordial follicles in an ELAVL2-dependent manner. To investigate the potential importance of the P-body-like granules for primordial follicle formation, we focused on *Ddx6*, a target gene of ELAVL2 that encodes a central component of P-body assembly [26,27]. We found that *Ddx6* is required for the assembly of the P-body-like granules and the formation of quiescent primordial follicles. Our study provides a framework to understand the molecular basis of the post-transcriptional network underlying the formation of primordial follicles.

## Results

### Identification of ELAVL2 as a candidate RNA-binding protein involved in the formation of primordial follicles

Primordial follicles are formed in neonatal ovaries. To explore the genes encoding RNA-binding proteins (RBPs) involved in the formation of primordial follicles, we performed a microarray analysis using total RNA isolated from embryonic day (E) 15.5, 17.5, and newborn (P0) ovaries, and selected relevant genes whose expression increased by more than twofold from E15.5 to P0. As a result, 55 gene probes encoding RBPs (GO: 0003723) were selected (Fig EV1A). We further focused on 17 genes among the 55 genes whose expression increased by more than twofold from E17.5 to P0, of which three genes, *G3bp2*, *Elavl2*, and *Dppa5*, had the strongest expression in the P0 ovary (Fig EV1B). As *Dppa5* knockout mice do not exhibit any abnormalities [28], *G3bp2* and *Elavl2* were selected to examine female-specific expression. Reverse transcription and quantitative polymerase chain reaction (RT-qPCR) revealed that *Elavl2* was predominantly expressed in the ovary, whereas *G3bp2* was increased toward birth not only in the ovary but also in the testis (Fig EV1C). As primordial follicle formation is a female-specific developmental event, we selected *Elavl2* as a strong candidate. Immunostaining analysis demonstrated that ELAVL2 was specifically expressed in oocytes marked by c-KIT (Fig EV1D). The specificity of the antibodies is shown in Fig 1C.

### *Elavl2* is indispensable for primordial follicle formation

ELAVL2 is a member of the ELAVL RNA-binding proteins (ELAVL1–4), which contain three RNA recognition motifs and associate with

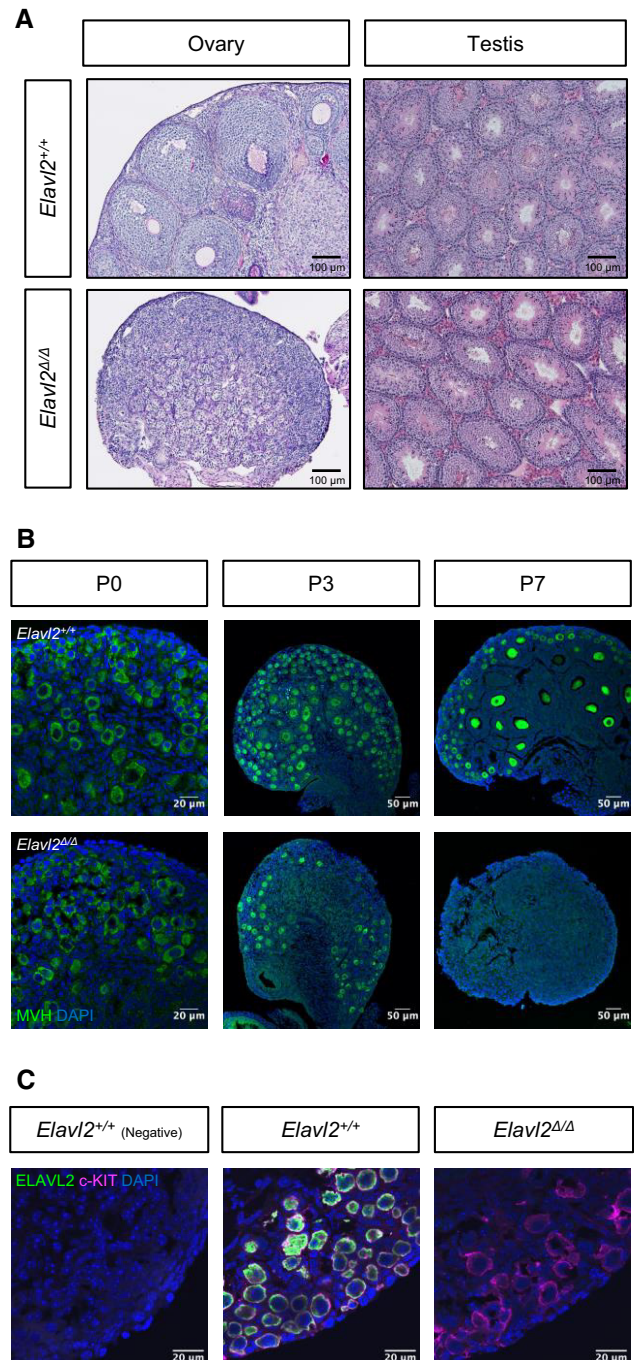


**Figure 1. Loss of oocytes shortly after birth in *Elavl2*-deficient ovaries.**

**A** Periodic acid–Schiff (PAS) staining in wild-type (*Elavl2*<sup>+/+</sup>) and *Elavl2* knockout (*Elavl2*<sup>Δ/Δ</sup>) adult ovaries (left) and testes (right) ( $n = 3$  animals for each genotype).  
**B** Immunostaining of a germ cell marker, MVH/DDX4, in neonatal ovaries ( $n = 3$  animals for each genotype). DNA was counterstained with 4',6-diamidino-2-phenylindole (DAPI).  
**C** Immunostaining of ELAVL2 newborn ovaries ( $n = 2$  animals for each genotype). Negative; negative control.

mRNAs containing AU-rich elements. ELAVL family proteins are involved in several post-transcriptional events, including alternative splicing, mRNA stability, and translation in somatic cells [29]. To

examine the role of ELAVL2 in the formation of primordial follicles, we generated *Elavl2* knockout mice (Appendix Fig S1A and B). Whereas a previous report indicates that ELAVL2 has oocyte-specific isoforms [30], Western blot analysis revealed that our *Elavl2* knockout mice were null mutants (Appendix Fig S1C). *Elavl2* knockout mice (*Elavl2<sup>A/A</sup>*) were born according to the Mendelian inheritance (Appendix Fig S1D). Although more than 80% of homozygous mutants progressively died by the weaning stage due to growth retardation (Appendix Fig S1E), the surviving pups grew to adulthood. We found that *Elavl2* knockout ovaries were markedly small in size and oocytes were lost in adults, whereas mutant testes exhibited no clear abnormalities in morphology (Fig 1A). To determine the cause of the ovarian defects, a time-course immunostaining analysis was conducted on *Elavl2* knockout neonatal ovaries using mouse vasa homolog (MVH, also known as DDX4) as a germ cell marker. The specificity of the antibody was shown (Appendix Fig S2A). We found that *Elavl2* knockout ovaries progressively lost oocytes after birth and oocytes were hardly observed in mutant ovaries at a week after birth (Fig 1B), indicating that *Elavl2* is required for the survival of oocytes in neonatal ovaries. Immunostaining analysis confirmed that ELAVL2 expression was not detected in mutant ovaries (Fig 1C).

We then asked whether cyst breakdown occurs in *Elavl2* knockout ovaries. To distinguish oocytes in cysts from those in primordial follicles, we performed immunostaining for an extracellular matrix protein, LAMININ (Fig 2A). The specificity of the antibodies was shown (Appendix Fig S2B). Primordial follicle formation began in the medullary area indicated by the LAMININ layer that encloses a single oocyte and surrounding granulosa cells (Fig 2A, asterisks), whereas oocytes in the cortical area were still connected with each other, represented by LAMININ-enclosed cysts in wild-type newborn ovaries (Fig 2A, dashed circles). On the other hand, primordial follicles were hardly observed in the medullary area, represented by LAMININ-enclosed oocytes that were broadly observed in *Elavl2* knockout ovaries (Fig 2A). We next examined the number of intercellular bridges (ICBs), cell junctions that connect oocytes in cysts, by performing immunostaining for the ICB markers TEX14 and MKLP1 [31] (Fig 2B). ICBs were detected as small dot- or ring-like signals as indicated by white arrowheads (Fig 2B). We confirmed that these small foci were specifically observed in a first antibody-dependent manner (Appendix Fig S2C). Quantification of TEX14 and MKLP1 foci revealed that the number of ICBs was approximately doubled in *Elavl2* knockout ovaries (Fig 2C). These results indicated that cyst breakdown is severely compromised in *Elavl2* knockout ovaries.

To evaluate the influence of *Elavl2* deficiency on gene expression, we performed a time-course microarray analysis by extracting total RNA from *Elavl2* knockout E15.5, E17.5, and P0 ovaries. We found that gene expression (more than twofold difference) was greatly changed in mutant P0 ovaries (946 gene probes, Fig 2D), consistent with the timing of primordial follicle formation, in which the number of decreased gene probes (646) was approximately double that of increased gene probes (300) (Datasets EV1 and EV2). Among the decreased gene probes, representative genes involved in folliculogenesis (*Gdf9*), zona pellucida formation (*Zp1*, *Zp2*, and *Zp3*), and early zygotic development (*Npm2* and *Zar1*) were included (Fig 2E) [32–37]. These genes were reported to be directly or indirectly up-regulated by the oocyte-specific

transcription factors FIGLA or NOBOX [5,38]. RT-qPCR data revealed that *Figla* and *Nobox* expression was also decreased in *Elavl2* knockout ovaries together with a greater reduction of their downstream genes, including *Bmp15* and *Rfpl4* [38] (Fig 2F). We normalized the data using *Mvh* because its expression level in *Elavl2* knockout P0 ovaries was similar to wild-type in our microarray data (fold change: 1.02) and RT-qPCR (Ct values:  $25.27 \pm 0.39$  in wild-type and  $25.23 \pm 0.64$  in *Elavl2* knockout ovaries). As expression of these genes increased toward birth (Fig 2E), we further examined the influence of *Elavl2* deficiency on the expression of cognate genes. Among 735 gene probes whose expression increased from E17.5 to P0 in wild-type ovaries, more than half (418 gene probes, 56.9%) demonstrated decreased expression in *Elavl2* knockout P0 ovaries (Fig 2G). These data suggest that *Elavl2* deficiency globally influences oocyte gene expression. Based on the results of immunostaining and gene expression analysis, we concluded that ELAVL2 is an indispensable RBP involved in the formation of primordial follicles.

#### ELAVL2 associates with mRNAs encoding components of P-bodies, which assembled in oocytes prior to the formation of primordial follicles

To search for possible targets of ELAVL2, we performed RNA immunoprecipitation followed by sequencing (RIP-seq) analysis using wild-type newborn ovaries. Western blot analysis confirmed successful immunoprecipitation of ELAVL2 (Fig 3A). As a result, 2519 genes were identified as putative ELAVL2-associating mRNAs according to our stringent criteria (IP/input > 2,  $q$ -value <  $10^{-10}$ , Dataset EV3). Using this gene list, gene ontology analysis was carried out to explore the cellular events that ELAVL2-associating mRNAs are involved in. Although ELAVL2-associated mRNAs were varied in terms of molecular or cellular events, we found that four terms related to RNA processing were included in the top 10 of the list (Fig 3B), among which three terms (CCR4-NOT, cytoplasmic stress granule, and cytoplasmic processing body) were related to cytoplasmic ribonucleoprotein (RNP) granules (Dataset EV4).

Cytoplasmic RNP granules are membraneless biomolecular condensates induced by liquid-liquid phase separation [39]. Accumulating evidence has demonstrated that these RNP granules are closely associated with numerous biological processes, including cell survival, neurodegenerative diseases, and germline development [40–42]. We thus hypothesized that primordial follicle formation involves ELAVL2-directed regulation of cytoplasmic RNP granules. To address this question, we first investigated the subcellular localization of cytoplasmic RNP granules in perinatal oocytes by focusing on a DEAD-box RNA helicase, DDX6, because DDX6 is a component of both P-bodies [26,27] and stress granules [43]. We found that DDX6 formed aggregate-like foci in newborn oocytes (Fig 3C, arrowheads), whereas it was diffused in the oocyte cytoplasm at E17.5 (Fig 3C). The stage-specific existence of granular signals was confirmed by immunostaining of negative control (Appendix Fig S3A). The number of oocytes containing clear DDX6 foci increased toward birth (Fig 3D), suggesting that DDX6-containing RNP granules are assembled prior to the formation of primordial follicles. DDX6 foci were also observed in oocytes after primordial follicles had formed (Fig 3E, arrows); however, their size was slightly smaller than those in cysts (Fig 3E, arrowheads). Thus,

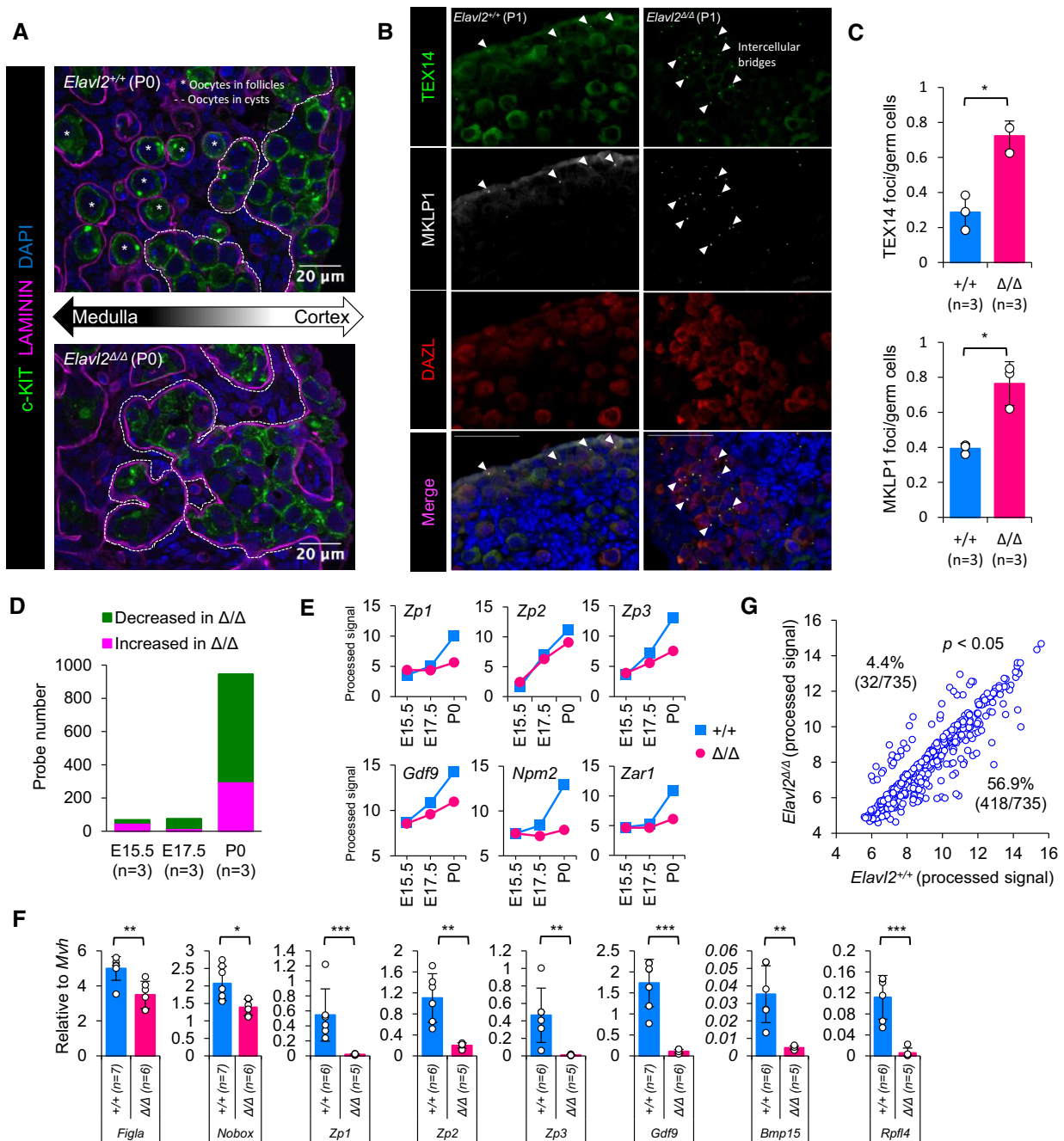


**Figure 2. *Elavl2* is indispensable for primordial follicle formation.**

A Immunostaining of an extracellular matrix protein, LAMININ, and a germ cell marker, c-KIT in wild-type (*Elavl2*<sup>+/+</sup>) and *Elavl2* knockout (*Elavl2*<sup>Δ/Δ</sup>) newborn ovaries (n = 3 animals for each genotype).  
 B Immunostaining of TEX14 and MKLP1 in newborn ovaries (n = 3 animals for each genotype). Oocytes were marked by DAZL. Scale bars, 50 μm.  
 C Quantification of TEX14 and MKLP1 foci (n = 3 animals) in (B).  
 D Microarray analysis of wild-type (WT) and *Elavl2* knockout ovaries (n = 3 independent ovary samples). Gene probes up- or down-regulated by more than twofold in *Elavl2* knockout ovaries are shown.  
 E Expression profile of selected genes involved in follicular and early zygotic development in (D).  
 F Reverse transcription and quantitative polymerase chain reaction (RT-qPCR) of selected genes (n = 5–7 animals).  
 G Scatter plot analysis of gene probes whose expression increased by more than twofold from E17.5 to P0 in WT ovaries in (D). Probes demonstrating a greater than 1.5-fold difference between wild-type and *Elavl2* knockout ovaries are shown.

Data information: (C, F, and G) Circles indicate individual data. Error bars, ±SD. The significance is indicated (two-tailed Student's t-test; \*\*\*P < 0.0005, \*\*P < 0.005, \*P < 0.05).

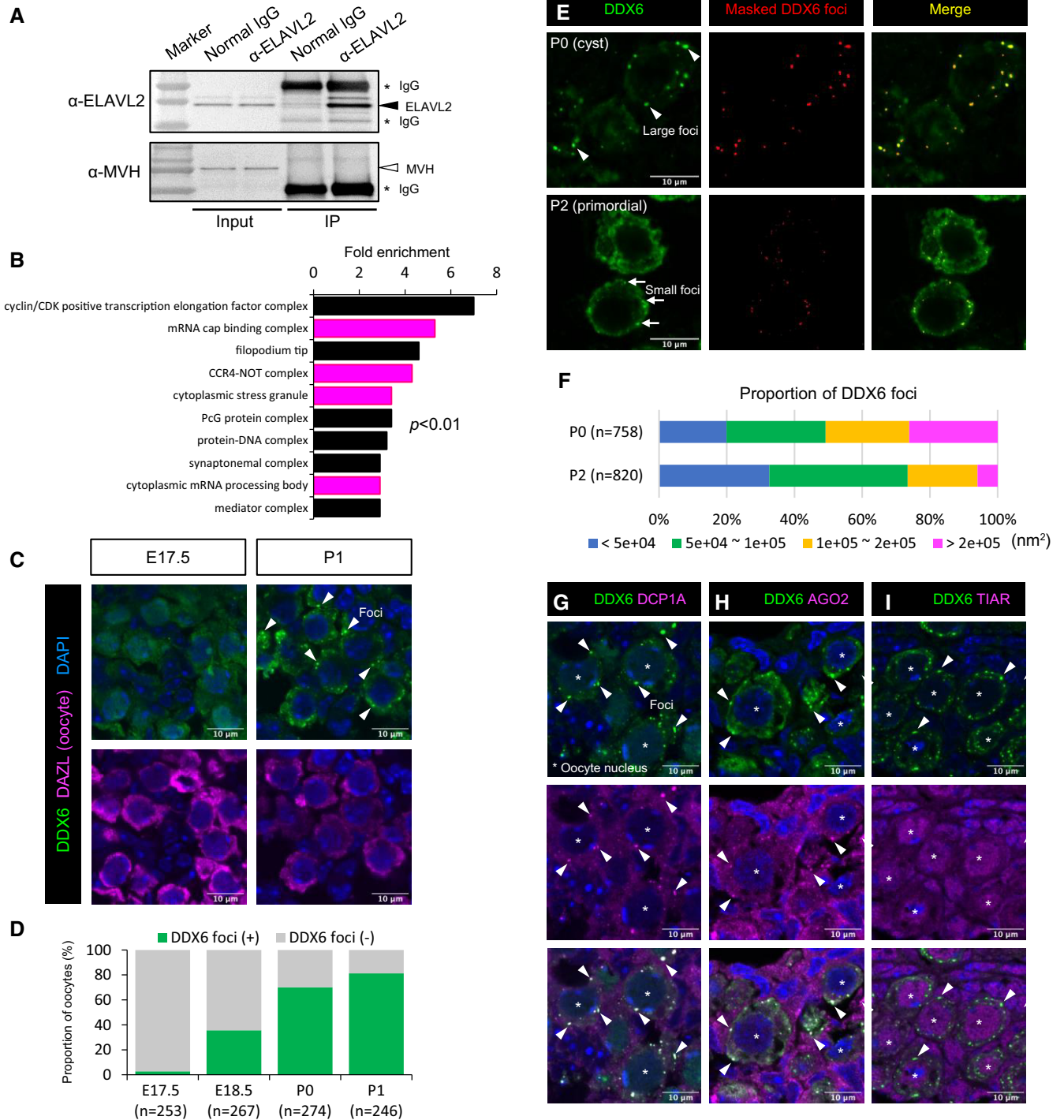


**Figure 3. ELAVL2 associates with mRNAs encoding components of P-bodies that assembled in oocytes prior to the formation of primordial follicles.**

- A** RNA immunoprecipitation of ELAVL2 using WT newborn ovaries. Immunoprecipitated ELAVL2 was confirmed by Western blotting. MVH was used as a negative control ( $n = 3$  independent ovary samples).
- B** Gene ontology analysis (DAVID ver. 6.8) of ELAVL2-associating mRNAs.
- C** Immunostaining of DDX6 in E17.5 ( $n = 3$  animals) and P1 ( $n = 10$  animals) ovaries. DAZL was used as an oocyte marker.
- D** Quantification of oocytes containing DDX6 foci ( $n =$  number of oocytes from two animals at each stage).
- E** Images analysis of DDX6 foci. Images of DDX6 from P0 and P2 ovaries (left) were used to create masks of DDX6 foci (middle). Merged images are shown on the right.
- F** Quantification of DDX6 foci ( $n =$  number of oocytes from two animals at each stage).
- G–I** Immunostaining of DCP1A (**G**) ( $n = 6$  animals), AGO2 (**H**) ( $n = 3$  animals), and TIAR (**I**) ( $n = 5$  animals) together with DDX6 in newborn ovaries. DNA was counterstained with DAPI.

we quantified their size by image analysis (Fig 3E, middle) and found that the proportion of large foci decreased in primordial follicles (Fig 3F, magenta). Instead, smaller foci became more abundant in primordial follicles (Fig 3F, blue and green). We next performed co-immunostaining using antibodies for P-body components, DCP1A [44,45] and AGO2 [46,47], and a stress granule component, TIAR [48], together with DDX6. As a result, DCP1A and AGO2, but not TIAR, colocalized to DDX6 foci in newborn oocytes (Fig 3G–I). The specificity of the antibodies was represented by DCP1A (Appendix Fig S3B). These results demonstrate that large P-body-like granules were assembled in oocytes prior to the formation of primordial follicles.

### ELAVL2-dependent DDX6 translation is required for the assembly of P-body-like granules

We next analyzed the assembly of P-body-like granules in *Elavl2* knockout newborn ovaries. Immunostaining of P-body components revealed that the assembly of P-body-like granules was impaired in *Elavl2* knockout ovaries (Fig 4A and B). To quantitatively analyze the results of immunostaining, we performed image analysis and measured the area of DDX6 foci per unit area of oocytes ( $1 \mu\text{m}^2$ ). The area of DDX6 foci was decreased to approximately one-fourth in *Elavl2* knockout ovaries (Fig 4C), indicating that massive assembly of P-body-like granules requires ELAVL2 function. The expression changes in mRNAs related to P-body were less than twofold in *Elavl2* knockout P0 ovaries (Fig 4D), suggesting that ELAVL2 has little effect on mRNA stability. We then examined protein expression by focusing on DDX6 as a model. According to Western blot analysis, DDX6 expression in *Elavl2* knockout ovaries decreased to 34% of that in wild-type (Fig 4E), suggesting that ELAVL2 is required for the translation or stability of DDX6. In addition, DCP1A and AGO2 expression appeared to be weaker in *Elavl2* knockout ovaries (Fig 4A and B). Although we could not detect their expression changes by Western blotting due to high backgrounds, it is possible that ELAVL2 broadly influences for protein expression of the components of P-body-like granules.

To further clarify the interaction between ELAVL2 and *Ddx6* mRNA, Flag-tagged ELAVL2 was transfected into HeLa cells together with a *gfp* reporter (Fig 4F). Successful expression and immunoprecipitation of ELAVL2 was confirmed by Western blotting (Fig 4G). RT-qPCR analysis revealed that interaction between ELAVL2 and the *gfp* reporter was greatly increased in a *Ddx6* 3'-UTR sequence-dependent manner (Fig 4H). ELAVL family proteins have three conserved RNA recognition motifs (RRM1-3), among which RRM1 and RRM2 cooperatively bind to AU-rich elements [49]. To test the role of RRM1 and RRM2 in the binding of the 3'-UTR sequence of *Ddx6*, mutant ELAVL2, which carried a large deletion in RRM1 and RRM2, was transfected (Fig 4F and G). We found that the interaction was diminished to one-tenth in the RRM mutant (Fig 4H). These data suggest that ELAVL2 is involved in the translation of DDX6 by directly associating with its 3'-UTR sequence.

### DDX6 is required for the assembly of P-body-like granules and the formation of primordial follicles

The defective assembly of P-body-like granules in *Elavl2* knockout ovaries prompted us to ask the importance of the ELAVL2-directed

assembly of P-body-like granules for the formation of primordial follicles. To address this question, we knocked out *Ddx6* in an oocyte-specific manner using *Mvh-Cre* [50] based on the requirement of DDX6 for P-body assembly in somatic cells [26] (Appendix Fig S4A and B). Hereafter, we refer to this mouse line as *Ddx6* cKO. On immunostaining analysis of P-body components, the assembly of P-body-like granules was severely compromised in *Ddx6* cKO newborn oocytes (Fig 5A and B). Quantification of DCP1A foci by image analysis revealed that the mean area of foci was reduced to 15% in *Ddx6* cKO ovaries (Fig 5C). As ELAVL2 was robustly expressed in *Ddx6* cKO oocytes (Fig 5D), it is unlikely that the defective assembly of P-body-like granules was due to the reduction of ELAVL2. These results indicate that *Ddx6* is required for the assembly of P-body-like granules.

We next examined the consequences of *Ddx6* deficiency for primordial follicle formation. Histological analysis demonstrated that approximately half of the oocytes remained in cysts in *Ddx6* cKO ovaries even at 7 days after birth (Fig 5E and F, dashed circles, and Fig 5G), whereas most oocytes had developed to primordial follicles in normal ovaries (Fig 5E and F, arrowheads, and Fig 5G). Direct connection between oocytes was shown by immunostaining for a germ cell marker, CDH1 (Fig 5F, dashed circles). The specificity of antibodies was shown (Appendix Fig S5A). Accordingly, the number of growing follicles (follicles in the transition state, T, primary follicles, PF, and secondary follicles, SF) was reduced in *Ddx6* cKO ovaries (Fig 5G). These data indicate that *Ddx6* is required for normal formation of primordial follicles. Furthermore, expression levels of genes regulated by FIGLA and NOBOX were decreased in *Ddx6* cKO ovaries, whereas those of *Figla* and *Nobox* themselves were increased (Fig 5H), suggesting that the oocyte gene expression program is primed but impaired in *Ddx6* cKO ovaries. Taken together, these results support the idea that primordial follicle formation involves ELAVL2-directed assembly of P-body-like granules.

### DDX6 ensures quiescence of primordial follicles by attenuating PI3K-AKT signaling

Although cyst breakdown was severely compromised, a substantial amount of primordial follicles developed in *Ddx6* cKO ovaries. To investigate the terminal phenotype, *Ddx6* cKO females were crossed with wild-type males, demonstrating that *Ddx6* cKO females were infertile and oocytes were lost in adult ovaries (Fig 6A and B). Of note, primordial follicles were abnormally enlarged at 2 weeks after birth (Fig 6C, red arrowheads). Quantification analysis revealed that the diameter of oocytes in primordial follicles was 1.3-fold longer in *Ddx6* cKO ovaries (Fig 6D). Primordial follicles were hardly observed by 3 weeks after birth in *Ddx6* cKO ovaries (Fig 6C and E). Accordingly, the number of growing follicles was greatly reduced (Fig 6E). This may account for the female infertility. We noticed that the abnormal enlargement of primordial follicles in *Ddx6* cKO ovaries resembled that observed in postnatal oocyte-specific knockout mice for *Pten*, a suppressor of PI3K-AKT signaling [51]. The removal of *Pten* in primordial follicles results in the up-regulation of PI3K-AKT signaling, which induces premature oocyte enlargement. Because the activation of PI3K-AKT signaling can be monitored by nuclear to cytoplasmic translocation of FOXO3A transcription factor [52], we performed immunostaining for FOXO3A and examined the

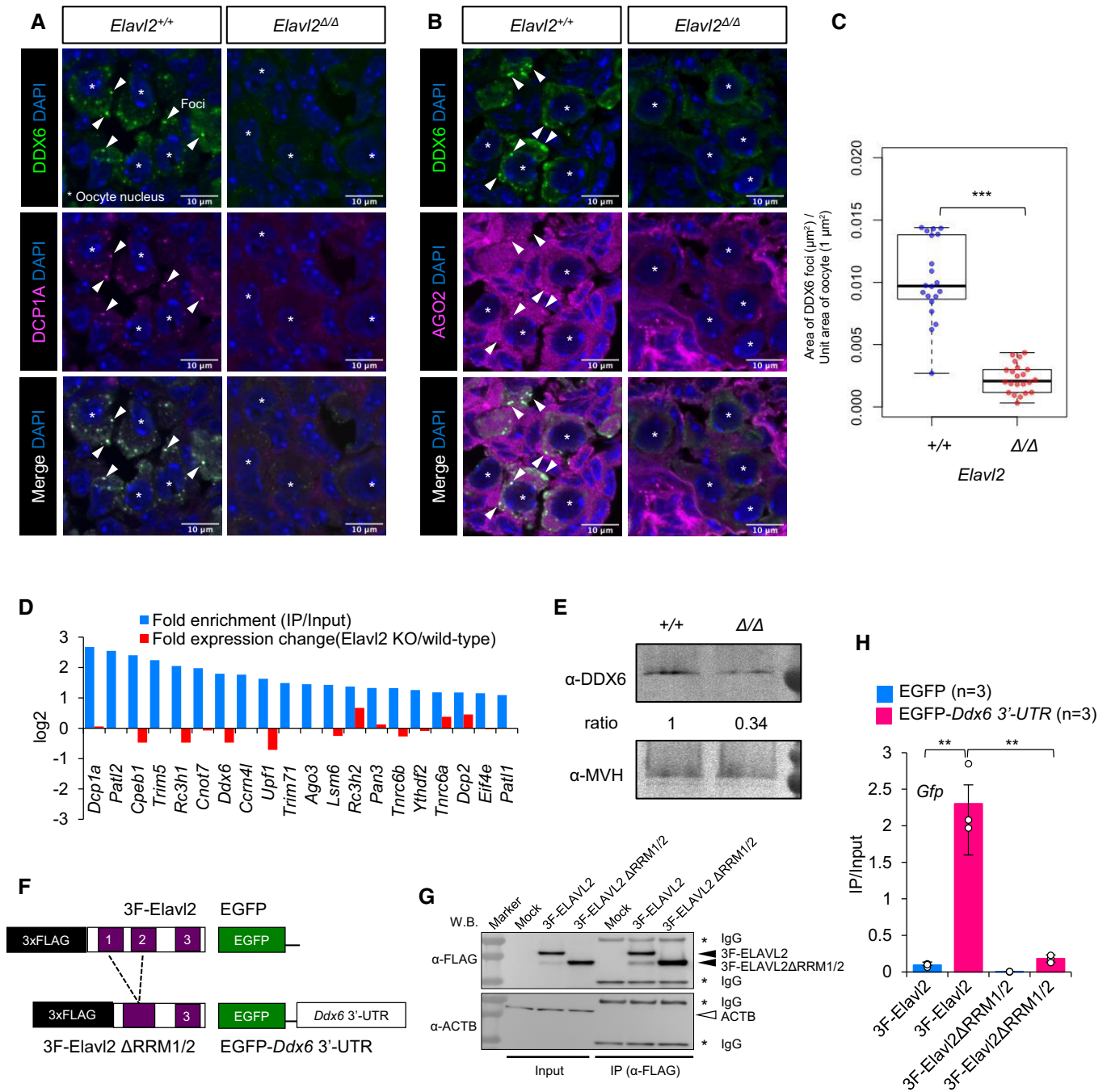


**Figure 4. ELAVL2-dependent DDX6 translation is required for the assembly of P-body-like granules.**

A, B Immunostaining of DDX6 together with DCP1A (A) (*n* = 6 animals for each genotype) and AGO2 (B) (*n* = 3 animals for each genotype) in wild-type (*Elavl2*<sup>+/+</sup>) and *Elavl2* knockout (*Elavl2*<sup>Δ/Δ</sup>) newborn ovaries.

C Quantification of the area of DDX6 foci in newborn ovaries. Twenty (wild-type) and 21 (*Elavl2* knockout) ovarian sections from two animals were immuno-stained by anti-DDX6 antibody and analyzed.

D Expression changes of mRNAs encoding components of P-bodies. Blue bars, fold enrichment of ELAVL2-associating mRNAs in Fig 3B. Red bars, fold expression changes of cognate mRNAs by microarray (P0 ovaries).

E Western blotting of DDX6 in newborn ovaries. The expression level of DDX6 in *Elavl2* knockout ovaries was normalized by MVH and represented as a ratio to WT.

F Co-transfection assay of full-length and mutant ELAVL2 with *gfp* reporters in HeLa cells.

G Detection of immunoprecipitated ELAVL2 by Western blotting. ACTB was used as a negative control.

H RT-qPCR analysis of *gfp* reporters. The vertical axis indicates relative quantity of immunoprecipitated *gfp* to inputs (*n* = number of experiment).

Data information: (C and H) Circles represent individual data. Error bars, ±SD. Boxes and horizontal bands in boxes represent quartile deviations and median, respectively. The significance of changes is indicated (Wilcoxon rank sum test in (C) and two-tailed Student's *t*-test in (H); \*\*\**P* < 0.0005, \*\**P* < 0.005).

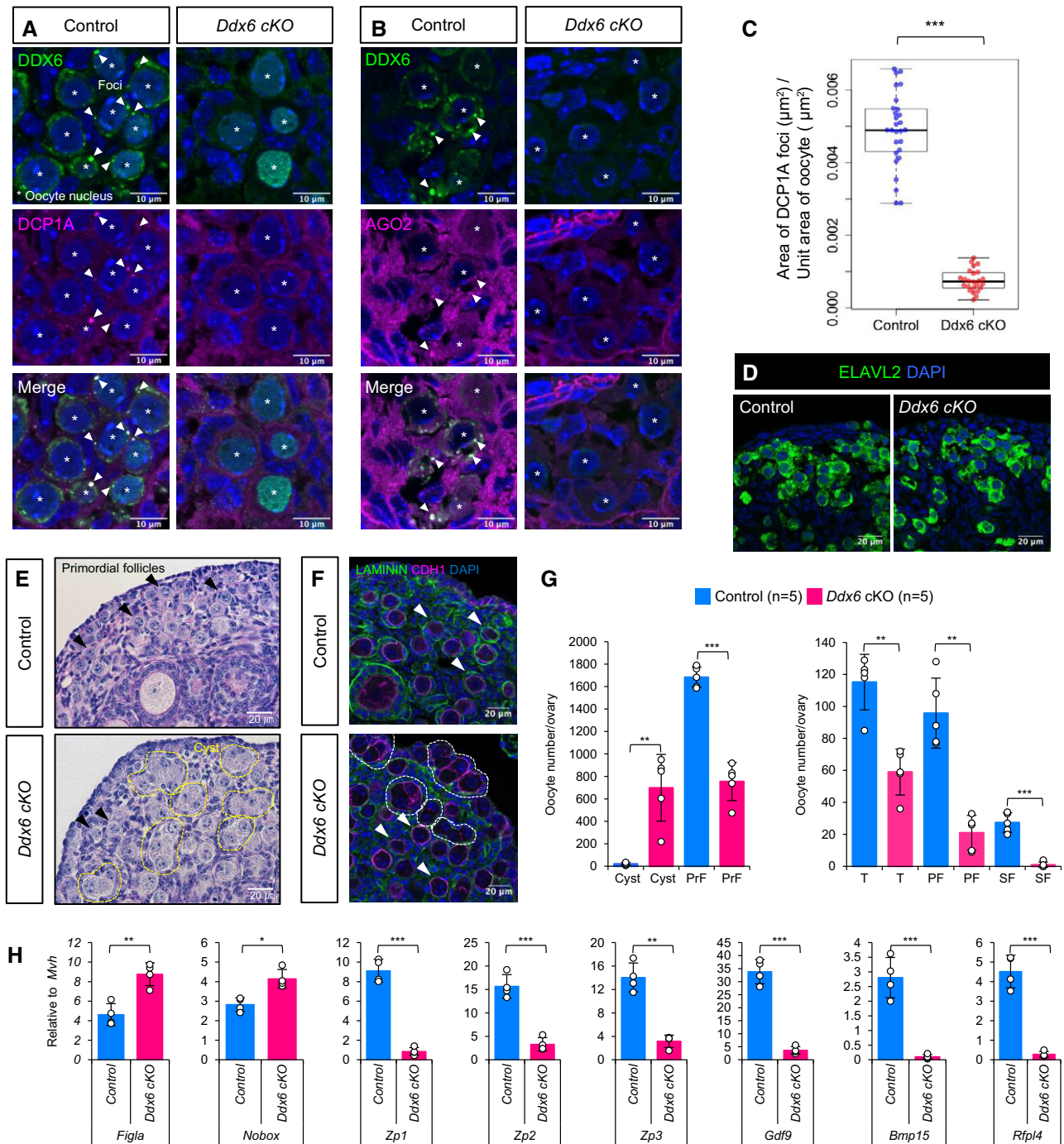


**Figure 5. DDX6 is required for the assembly of P-body-like granules and the formation of primordial follicles.**

A, B Immunostaining of DDX6 together with DCP1A (A) ( $n = 3$  animals for each genotype) and AGO2 (B) ( $n = 3$  animals for each genotype) in newborn ovaries. DNA was counterstained with DAPI.  
 C Quantification of the area of DCP1A foci in newborn ovaries. Twenty-eight (control) and 25 (*Ddx6* cKO) ovarian sections from two animals were immuno-stained by anti-DCP1A antibody and analyzed.  
 C Immunostaining of ELAVL2 in newborn ovaries ( $n = 3$  animals for each genotype).  
 E PAS staining of P7 ovaries ( $n = 5$  animals for each genotype).  
 F Immunostaining of an oocyte marker, CDH1, together with LAMININ in P7 ovaries ( $n = 3$  animals for each genotype).  
 G Oocyte counting analysis of P7 ovaries ( $n =$  animals). Cyst, oocyte in cyst; PrF, primordial follicle; T, transition; PF, primary follicle; SF, secondary follicle.  
 H RT-qPCR analysis of P7 ovaries ( $n = 4$  animals).

Data information: (C, G, and H) Circles indicate individual data. Error bars,  $\pm$ SD. Boxes and horizontal bands in boxes represent quartile deviations and median, respectively. The significance of changes is indicated (Wilcoxon rank sum test in (C) and two-tailed Student's *t*-test in (G and H); \*\*\*\* $P < 0.0005$ , \*\*\* $P < 0.005$ , \* $P < 0.05$ ).



activation state of PI3K-AKT signaling in *Ddx6* cKO ovaries. Consistent with a previous observation [52], FOXO3A was localized to the cytoplasm in cysts and its nuclear translocation coincided with the

formation of primordial follicles in normal ovaries (Fig 6F, P1, P7). On the other hand, nuclear translocation of FOXO3A was not observed in *Ddx6* cKO newborn oocytes (Fig 6F, P1) and it

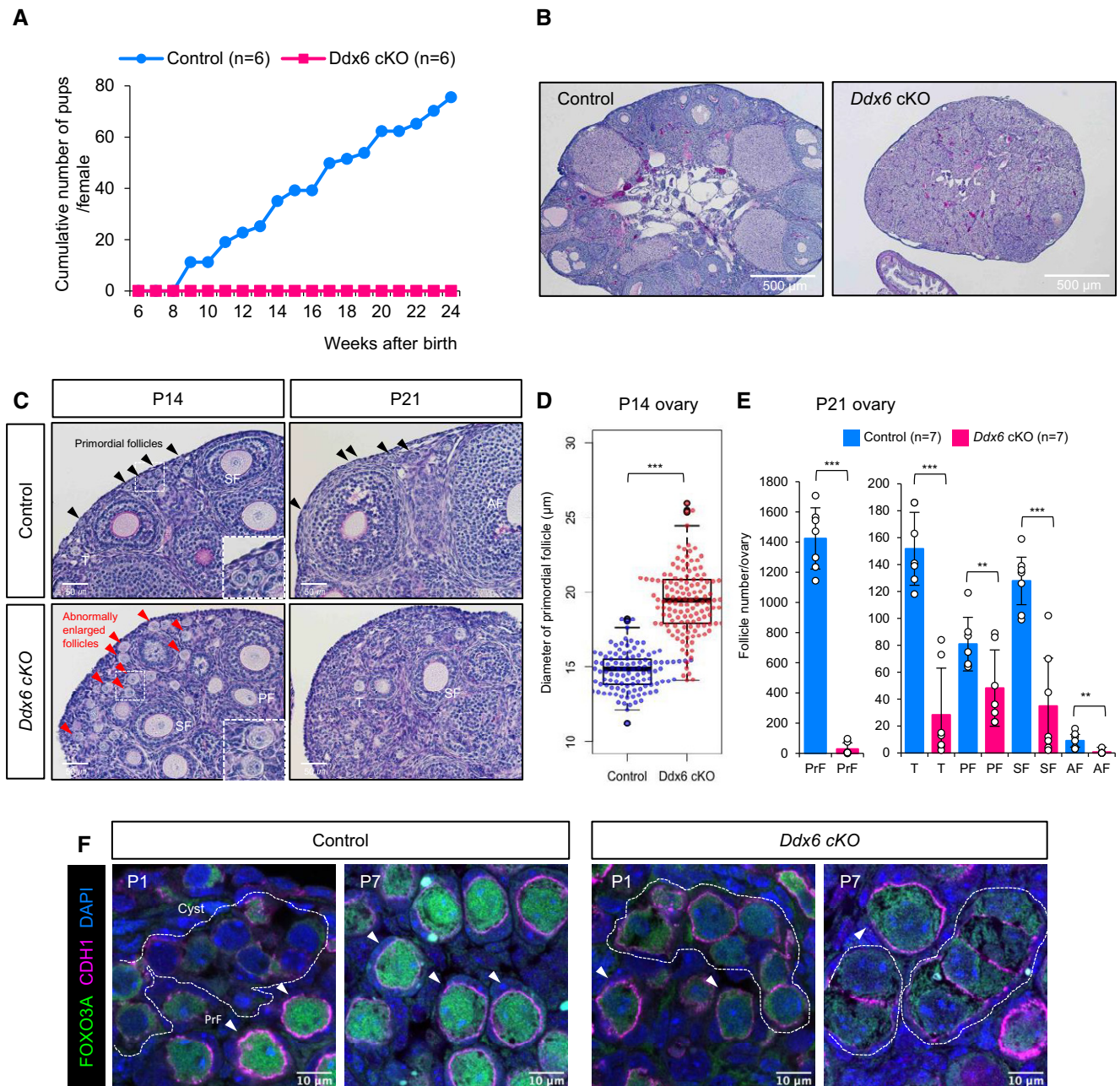


**Figure 6. DDX6-dependent attenuation of PI3K-AKT signaling is involved in the formation of primordial follicles.**

A Litter size analysis of *Ddx6* cKO females. *Ddx6*<sup>+/+</sup>, *Ddx6*<sup>+/+</sup>; *Muh-Cre*, and *Ddx6*<sup>lox/+</sup> females were used as control. Control and *Ddx6* cKO females (*n* = 6 animals for each genotype) were crossed with wild-type males from 6 to 24 weeks after birth.

B PAS staining of adult *Ddx6* cKO ovaries (*n* = 6 animals for each genotype).

C PAS staining of P14 (*n* = 3 animals) and 21 (*n* = 7 animals) ovaries. Areas indicated by white squares are magnified. T, transition; PF, primary follicle; SF, secondary follicle; AF, antral follicle.

D Quantification of the oocyte diameter for primordial follicles in P14 ovaries. Data were obtained from two animals for each genotype.

E Oocyte counting analysis for P21 ovaries (*n* = 7 animals for each genotype). T, PF, and SF are the same as in Fig 5G. AF, antral follicle.

F Immunostaining of FOXO3A and CDH1 in P1 and 7 ovaries (*n* = 3 animals for each genotype). PrF, primordial follicle.

Data information: (D and E) Circles indicate individual data. Error bars,  $\pm$ SD. Boxes and horizontal bands in boxes represent quartile deviations and median, respectively. The significance of changes is indicated (Wilcoxon rank sum test in (D) and two-tailed Student's *t*-test in (E); \*\*\**P* < 0.0005, \*\**P* < 0.005).

remained in cytoplasm in P7 ovaries (Fig 6F, P7). The specificity of antibodies was shown (Appendix Fig S5B). These data indicate that DDX6 is required for the attenuation of PI3K-AKT signaling in primordial follicles and account for abnormal enlargement of primordial follicles in *Ddx6* cKO ovaries.

## Discussion

The formation of primordial follicles proceeds within a relatively short time period in perinatal ovaries. Although transcription factors and signaling molecules involved in primordial follicle formation have been reported [5–9], the importance of post-transcriptional gene regulation has not been addressed. In this study, we identified ELAVL2 as an essential RBP required for the formation of primordial follicles. Through the analysis of *Ddx6* as an important target of ELAVL2, we revealed an ELAVL2-dependent molecular network to be involved in the assembly of P-body-like granules and the formation of primordial follicles. Furthermore, this molecular network ensures the quiescence of primordial follicles by attenuating PI3K-AKT signaling, a signaling pathway responsible for controlling oocyte size. We propose that ELAVL2 directs an important post-transcriptional network that drives the formation of quiescent primordial follicles.

ELAVL family proteins are one of the RBPs whose molecular function has been extensively investigated. As ELAVL RNA-binding proteins are orthologs of *Drosophila* *Elav* (*embryonic lethal abnormal vision*), most studies were conducted to address their functions in neural cells or related cell types. In this study, we identified ELAVL2 as an indispensable factor for the formation of primordial follicles in the mouse ovary. At the molecular level, ELAVL2 associates with a variety of mRNAs, including those encoding cytoplasmic RNP granules, among which our results revealed the importance of ELAVL2-dependent DDX6 translation. This is consistent with the reported molecular function of ELAVL2. According to the RNA operon (or regulon) hypothesis, mRNAs encoding functionally related proteins are coordinately regulated by relevant RBPs [53]. ELAVL2 may be one such RBP in oocytes. On the other hand, murine ELAVL2 was reported to act as a translational suppressor in growing oocytes [30]. It is possible that ELAVL2 plays multiple roles in a context- or developmental stage-dependent manner. To gain a deeper understanding of the molecular function of ELAVL2 in oocytes, studies on other ELAVL family proteins may be useful. For example, ELAVL4 was reported to enhance translational activity depending on its interaction with eIF4A and the poly (A) tail [54]. Whether ELAVL2 has similar characteristics to other ELAVL proteins is of interest. Furthermore, ELAVL2 has important target mRNAs other than *Ddx6* because the phenotype in *Elavl2* knockout ovaries was more severe than that in *Ddx6* cKO ovaries. Identification of such target RNAs will also facilitate our understanding of ELAVL2 and the mechanism of primordial follicle formation.

We found that large P-body-like granules were assembled in oocytes prior to the formation of primordial follicles in an ELAVL2-dependent manner. The granules also exist in primordial follicles but their size became smaller. The potential importance of the P-body-like granules was suggested by oocyte-specific knockout of *Ddx6*. Considering the assembly of large P-body-like granules

together with the concept of liquid–liquid phase separation, it is likely that abundant mRNAs expressed in cysts are aggregated together with RBPs over the saturation constant. Whether mRNAs encoding proteins that function in cysts or those that function in primordial follicles are recruited to the large granules is an interesting question. On the other hand, a recent study reported that cytoplasmic organelle transport from nurse-like oocytes to the destined oocytes occurs during the formation of primordial follicles in mice, reminiscent of *Drosophila* oogenesis [55]. Considering evolutionary similarities, P-body-like granules in perinatal oocytes may function in the translational suppression of mRNAs during material transport. Moreover, recent studies demonstrated that cytoplasmic RNP granules sequestered mTORC1 (the targeted rapamycin complex) by trapping mTOR, a central protein kinase involved in PI3K-AKT signaling [56–58]. As PI3K-AKT signaling was abnormally activated in *Ddx6* cKO ovaries, P-body-like granules may exert such functions. To clarify the role of the temporal assembly of large P-body-like granules in cysts, methods to disturb granule assembly without affecting the molecular functions of the components are required.

We identified *Ddx6* as an important target of ELAVL2. DDX6 is an evolutionarily conserved DEAD-box RNA helicase involved in the translational suppression of maternal RNAs and oocyte survival in *Drosophila* and *Caenorhabditis elegans* [59,60]. Although the evolutionary importance of DDX6 family proteins in oocytes is known, its role in mammalian oocytes has not been addressed. We found that depletion of DDX6 in oocytes resulted in the defective formation of primordial follicles, which is the first demonstration of a physiological role of DDX6 in mammalian oogenesis. As the loss of DDX6 activates PI3K-AKT signaling, the defective formation of primordial follicles may be explained by abnormal enlargement of oocytes. How DDX6 attenuates PI3K-AKT signaling is an open question. Considering the molecular function of DDX6 family proteins as translational suppressors and the involvement of the receptor tyrosine kinase c-KIT in the activation of AKT signaling [61], DDX6 may suppress the translation of c-KIT or other proteins involved in the signal cascade. In addition to the attenuation of PI3K-AKT signaling, genes regulated by FIGLA and NOBOX were markedly decreased even in the presence of ELAVL2 in *Ddx6* cKO ovaries, indicating that DDX6 is more directly responsible for their expression. To clarify the role of DDX6 in the regulation of PI3K-AKT signaling and oocyte gene expression, identification of target mRNAs of DDX6 is required. Unveiling the molecular function of DDX6 may also facilitate our understanding of long-term reproduction of mammalian females because our data suggest that DDX6 is required for maintaining the quiescence state of primordial follicles.

Lastly, our study provides a framework to understand the molecular basis of post-transcriptional gene regulation involved in the formation and the maintenance of the quiescent state of primordial follicles. Knowledge from our and subsequent studies may aid in the production of quiescent primordial follicles *in vitro*, which will be useful not only for scientific research but also for medical and industrial applications. In this regard, recent papers from Hayashi's laboratory reported that hypoxia and mechanical stress play important roles in the formation and the maintenance of primordial follicles during this revision [62,63]. Taken together with these novel findings, further studies should be addressed to reveal the mechanisms of this developmental process.

## Materials and Methods

### Mice

Mice were housed in a specific-pathogen-free animal care facility at the National Institute of Genetics. All experiments were approved by the NIG Institutional Animal Care and Use Committee. *CAG-Cre*, *Mvh-Cre*, and *Rosa-Flp* mice used in this study were generated previously [50,64,65]. All mouse lines used in this study were of a mixed genetic background.

**Production of *Elavl2* conditional knockout mice:** For the targeting vector construction, homologous arms and exon 3 of *Elavl2* were prepared by PCR amplification from the mouse genome and were integrated into the DT-ApA/conditional KO FW vector containing the *loxP*, *Frt*, and *Pgk*-neomycin cassette (<http://www.cdb.riken.go.jp/arg/cassette.html>). The targeting vector was electroporated into TT2 ES cells, and the homologous recombinants were selected using 150 µg/ml neomycin-containing medium. Correctly recombined ES cells were screened using the following primer sets: ELAVL2-LAF3 (5'-GTGGATACTACAGGTAAGTGAG-3') and ELAVL2-E2R (5'-CAAGTTGGCCATTAGACAG-3') for 5' recombination, and Neo-pA-L1 (5'-GCTCATTCCTCCCACTCATG-3') and ELAVL2-SA-OUT-R1 (5'-TAGGGTGGCCACCGAGCAATTG-3') for 3' recombination. These ES cells were aggregated with 8-cell embryos, and the blastocysts that formed the next day were transferred to foster mothers to generate chimeric mice. After confirming germline transmission, the neomycin cassette was removed by crossing with *Rosa-Flp* mice.

**Production of *Ddx6* conditional knockout mice:** For targeting vector construction, the homologous arms and exon 5 of *Ddx6* were prepared by PCR amplification from the mouse genome and were integrated into a vector containing two *loxP* sequences via the sequential infusion method (the targeting vector sequence is available upon request). A *Pgk*-neomycin cassette flanked by two *Frt* sequences was then inserted upstream of the right arm. Two Cas9 target sites were selected using CRISPR direct (<http://crispr.dbcls.jp/>), and each target sequence was integrated into the px330 Cas9 vector (Addgene). These vectors were transfected into TT2 ES cells using Lipofectamine 2000 (Invitrogen), and homologous recombinants were selected using 150 µg/ml neomycin-containing medium. Accurately recombined ES cells were screened using the following primer sets: DDX6-GL1 (5'-CTCCCCTCTGGGATTTAGGG-3') and Lox-R1 (5'-TACGAAGTTATTAGGTCCTCGAAG-3') for 5' recombination, and PGK-R (5'-CTAAAGCGCATGCTCCAGACT-3') and DDX6-GR1 (5'-AAGTTTGAGGACAGCCAGGGC-3') for 3' recombination. These ES cells were aggregated with 8-cell embryos to generate chimeric mice as described above.

### Mouse breeding experiment

Control and *Ddx6* cKO females were crossed with wild-type (ICR) males when they reached 6 weeks of age. Each pair was kept in a breeding cage until the female mice became 24 weeks old, and the number of pups delivered during this period was counted.

### Antibodies

The antibodies used for immunofluorescence analysis and Western blotting are listed in Table EV1.

### Immunofluorescence staining

**Frozen samples:** Embryonic and newborn ovaries were fixed with 4% paraformaldehyde (PFA) in phosphate-buffered saline (PBS) for 0.5–1 h at 4°C. After washing with PBS, the fixed ovaries were infiltrated with 10 and 20% sucrose in PBS for 0.5–1 h at 4°C. The ovaries were then embedded in Tissue-Tek O.C.T. compound (Sakura Finetek, Japan) and frozen in liquid nitrogen. Ovaries were cryosectioned at 6 µm and applied to glass slides. After drying the cryosections and washing them in PBS, the glass slides were autoclaved in target retrieval solution (DAKO) at 105°C for 15 min and then pre-incubated with blocking buffer (3% skim milk and 0.05% Tween-20 in PBS) for 1 h at room temperature. The primary antibodies listed in Table EV1 were diluted in 0.05% Tween/PBS (PBST) and reacted overnight with the sections at 4°C. Negative controls of immunostaining were obtained by reacting sections with normal antibodies [normal goat/mouse/rabbit IgG (Santa Cruz, sc-2028/2025/3888), normal Armenian hamster/guinea pig IgG (MBL, M199-3/PM067)]. After washing the samples with PBST, secondary antibodies labeled with Alexa Fluor 488, 594, or 647 (1:1,000 dilution in PBST, Molecular probes) or Cy5 (1:1,000 dilution in PBST, Millipore) were reacted with the samples at RT for 1 h. DNA was counterstained using DAPI. Fluorescence micrographs were acquired using the Olympus FV1200 confocal microscope and processed with FV10-ASW (version 4.0) software.

**Paraffin-embedded samples:** Ovaries from 1-week-old mice were fixed overnight with 4% PFA/PBS at 4°C. After washing with PBS, the ovaries were dehydrated and embedded in paraffin wax following a standard protocol. The blocks were sliced at 6-µm thickness and placed on glass slides. After removing the paraffin wax and autoclaving in target retrieval solution at 105°C for 15 min, the glass slides were washed in PBS and pre-incubated in blocking buffer at RT for 1 h. The primary antibodies listed in Table EV1 were then diluted in PBST and reacted overnight with the sections at 4°C. Negative controls of immunostaining were obtained by reacting sections with normal antibodies as described above. After washing the samples with PBST, secondary antibodies labeled with Alexa 488 or 594 (1:1,000 dilution in PBST) were reacted with samples at RT for 1 h. DNA was counterstained with DAPI. Fluorescence micrographs were acquired using the Olympus FV1200 confocal microscope and processed with FV10-ASW (version 4.0) software.

For TEX 14 and MKLP1 staining, newborn ovaries embedded in paraffin were sectioned at 6-µm thickness and placed on glass slides. After removing the paraffin wax, samples were pre-incubated with 3% bovine serum albumin (Wako) in PBS at RT for 1 h. The samples were then reacted overnight with primary antibodies at 4°C. Negative controls of immunostaining were obtained by reacting sections with normal antibodies [normal goat/guinea pig/rabbit IgG (MBL, M094/PM067/PM035)]. After washing with PBST, the samples were reacted with secondary antibodies labeled with Alexa 488, 555, or 647 (Thermo Fisher Scientific, Bioss Antibodies) at RT for 1 h. DNA was counterstained with DAPI. Fluorescence micrographs were acquired using the Keyence BZ-X700 microscope and processed with the attached analyzer. For quantification, 2300 wild-type and 2201 *Elavl2* knockout oocytes were counted.

## Histological analysis

Histological analysis of ovarian sections from juvenile and adult mice was performed by periodic acid–Schiff (PAS) staining according to the standard protocol. Briefly, ovaries were fixed in Bouin's solution (Wako) and embedded in paraffin wax. Whole ovaries were sequentially sliced at 6- $\mu$ m thickness and submerged in xylene, followed by 100, 90, and 70% ethanol. After staining with hematoxylin and PAS solution, images were obtained using BX 51 and 61 microscopy (Olympus). The developmental stages of ovarian follicles were determined according to the criteria described in a previous study [66]. Follicles were counted on every five sections, and the oocyte diameter was measured using Cellsens software (Olympus).

## RT–qPCR

Total RNA was extracted from a pair of embryonic and newborn ovaries, and testes using RNeasy Mini Kits (Qiagen), and incubated with SuperScript III Reverse Transcriptase (Invitrogen) for 60 min at 50°C to synthesize cDNA according to the manufacturer's procedure. Oligo (dT) (500 ng) was used for cDNA synthesis. Quantitative PCR was performed using KAPA SYBR Fast qPCR Kits (Nippon Genetics) and Dice Real Time System Single Thermal Cycler (Takara). The primers used are listed in Table EV2.

## Western blotting

Newborn ovaries lysed in 1 $\times$ SDS sample buffer [75 mM Tris–HCl, pH 6.8, 1.2% sodium deoxycholate (SDS), 15% glycerol, 7% 2-mercaptoethanol, and 0.001% bromophenol blue] were boiled for 5 min, separated on SDS–polyacrylamide gels, and transferred to nitrocellulose membranes. After the membranes were submerged in blocking buffer [5% skim milk in TBST (Tris–HCl, pH 7.5, 150 mM NaCl, and 0.1% Tween-20)] at RT for 20 min, primary antibodies diluted in TBST were reacted with the membranes at RT for 1 h. After washing the membranes with TBST, the secondary antibodies, horse/goat anti-mouse/rabbit immunoglobulin G conjugated with horseradish peroxidase (1:2,000, Cell Signaling), were diluted in TBST and reacted with membranes at RT for 30 min. Signals were detected using the SuperSignal West Femto Chemiluminescent Substrate Kit (Thermo Scientific). Images were captured using the EZ-Capture MG chemiluminescence imaging system (Atto).

## Image analysis

To quantify the DDX6 or DCP1A foci, oocyte sections were subjected to immunostaining for DDX6 or DCP1A together with a germ cell marker, DAZL. Confocal images were taken with Olympus FV1200 confocal microscope with a 100 $\times$  oil-immersion objective lens, at a pixel resolution of 1,024  $\times$  1,024 and 1.5 $\times$  zoom setting. Captured images were analyzed automatically using a custom program written for the R software environment ([www.r-project.org](http://www.r-project.org)) with the EBImage packages [67]. Oocyte masks were created using the images of DAZL staining, in brief, by applying a Gaussian blur filter followed by local thresholding. Granular objects of DDX6 or DCP1A were detected by applying the different Gaussian filters followed by local thresholding, hole filling, and size selection. The area of DDX6

or DCP1A foci in oocytes and those per unit area of oocytes were calculated based on the pixel size.

## Cell culture experiments

The 3 $\times$ FLAG-ELAVL2-expressing vector was generated by inserting the *Elavl2*-coding sequence into the p3 $\times$ FLAG-CMV7.1 vector (Sigma-Aldrich). As *Elavl2* has oocyte-specific isoforms [30], cDNA was reverse-transcribed from the total RNA of postnatal ovaries. The deletion mutant of the 3 $\times$ FLAG-ELAVL2-expressing vector was generated using the In-Fusion HD Cloning System (Takara), whereby RNA recognition motifs 1 and 2 were disrupted using the following primer set: dRRM1/2-F (5'-AGAGACAAAATAACAGACAAGCGGATTGAGGCAGAAG-3') and dRRM1/2-R (5'-CTCAATCGCTTGTCTGTTATTTTGTCTTACAAGC-3'). An EGFP reporter was generated by inserting the *Ddx6* 3'-UTR sequence into the pEGFP-C2 vector (Clontech). One microgram of 3 $\times$ FLAG-ELAVL2 or its deletion mutant vector was transfected together with the same amount of the EGFP reporter with or without the *Ddx6* 3'-UTR into 3  $\times$  10<sup>5</sup> HeLa cells using Lipofectamine 2000 (Thermo Fisher Scientific) according to the manufacturer's protocol. At 24 h after transfection, the cells were dissociated using 0.15% trypsin and collected by centrifugation (180  $\times$  g at 4°C for 2 min). Cells were then homogenized in IP buffer (20 mM HEPES/KOH, pH7.5, 150 mM NaCl, 2.5 mM MgCl<sub>2</sub>, 0.1% NP-40, 1 mM dithiothreitol, 1 $\times$  protease inhibitor cocktail (Roche), and 100 U/ml RNase inhibitor (Takara)). After removing the debris by centrifuging the lysates (10,000  $\times$  g at 4°C for 10 min), the supernatant was incubated with magnetic beads conjugated to protein G (Invitrogen), which were pre-incubated with an anti-FLAG M2 antibody (1:200, Sigma-Aldrich, F3165) at 4°C for 2 h. The lysate-bead mixtures were then incubated at 4°C for 6 h with gentle rotation. The bead–antibody complexes were washed thrice with IP buffer and transferred to fresh 1.5-ml tubes. The complexes were washed again with IP buffer. The precipitated proteins and RNA were eluted by incubating the bead–antibody complexes with the elution buffer (IP buffer containing 0.5% SDS) at 70°C for 5 min. Input samples (5% of starting material) were taken from the centrifuged supernatants. Immunoprecipitation of 3 $\times$ FLAG-ELAVL2 and its mutant protein was evaluated by Western blotting using anti-FLAG M2 and anti-ACTB antibodies according to the procedure described above. To quantify the precipitated reporter RNAs, eluted samples were dissolved in TRIzol reagent (Invitrogen), and RNA was extracted according to the manufacturer's protocol. cDNA synthesis and RT–qPCR were then performed according to the procedure described above.

## Microarray analysis

The quality of total RNA extracted from the wild-type and *Elavl2* knockout embryonic and P0 ovaries ( $n = 3$ , respectively) using RNeasy Mini Kits (Qiagen) was determined using the 2100 Bioanalyzer (Agilent). Aliquots (200 ng) of the RNA were then reverse-transcribed and labeled with Cy3 using the Low RNA Input Linear Amplification Kit (Agilent). The Cy3-labeled complementary RNAs were hybridized to a Whole Mouse Genome Oligo Microarray (G4122F, Agilent) using the Gene Expression Hybridization Kit (Agilent). The microarrays were scanned using a Microarray Scanner System (G2565BA, Agilent), and the generated images were

processed using the Feature Extraction software (version 9.1, Agilent).

### RNA immunoprecipitation and sequencing (RIP-seq)

One hundred newborn ovaries (three replicates) were homogenized in IP buffer, and the debris was removed by centrifugation ( $10,000 \times g$  at  $4^\circ\text{C}$  for 10 min). The supernatants were incubated with magnetic beads conjugated to protein G (Invitrogen), which were pre-incubated with anti-ELAVL2 antibody ( $5 \mu\text{g}$ , Proteintech, 14008-1-AP) at  $4^\circ\text{C}$  for 2 h. Immunoprecipitation, elution, and isolation of precipitated RNAs were performed according to the procedure described above, and the quality of RNAs was evaluated using the 2100 Bioanalyzer (Agilent). Anti-sense RNAs were amplified using the TargetAmp 1-Round aRNA Amplification Kit 103 (Epicentre) according to the manufacturer's protocol, and sequence libraries were then generated using the KAPA Stranded mRNA-Seq Kit Illumina platform (KAPA Biosystems) according to the manufacturer's protocol. The resulting libraries were sequenced on the Illumina GAIIx (single end 36 base reads with TruSeq SBS kit v5 for GA., Illumina). These input and RIP sequenced reads were then quality checked, and any duplicated reads were discarded prior to mapping against the mouse genome reference (GRCm38/mm10) using TopHat2 (<https://ccb.jhu.edu/software/tophat/index.shtml>) [68]. During the mapping, multiple-aligned reads were also discarded. The output bam files from TopHat2 were processed by MACS2 callpeak (<https://github.com/taoliu/MACS>) [69] to estimate potential ELAVL2-associated sequences. The cut-off q-value for the callpeak was  $1e-7$ , and the nomodel option was on. The called significant ranges were finally annotated using ChIPpeakAnno (<https://www.bioconductor.org/packages/release/bioc/html/ChIPpeakAnno.html>) [70] together with biomaRt (<https://bioconductor.org/packages/release/bioc/html/biomaRt.html>) [71] packages in the R statistical computing environment (<https://www.r-project.org>). The reference database for the annotation was Ensembl (<https://www.ensembl.org/index.html>), and the dataset was `mmusculus_gene_ensembl` for identifying gene IDs.

### Statistical analysis

Comparison of two groups was performed by Student's *t*-test except those in image analysis, in which Wilcoxon rank sum test was performed. Data are represented by means  $\pm$  SD. The significance level of changes was represented by asterisks ( $***P < 0.0005$ ,  $**P < 0.005$ ,  $*P < 0.005$ ).  $C_t$  value in RT-qPCR was calculated by the second derivative maximum method, and the relative quantity of each mRNA was calculated using the  $\Delta\Delta C_T$  method. In microarray analysis, data were obtained from three independent samples and processed using the Subio Platform (version 1.17, Subio) as follows: All values  $< 1$  were replaced with 1, and the data were normalized to the 75<sup>th</sup> percentile. The differentially expressed genes were extracted from the datasets by fold expression change (more than twofold) and Student's *t*-test ( $P < 0.05$ ).

### Data availability

Microarray and RNA-sequencing data are available in the Gene Expression Omnibus (GEO) database (Accession No: GSE112275

and GSE113305). Requests for material transfer should be made to Y.K. or Y.S. The custom program of image analysis is available from the following web site (<https://github.com/yukatonig/DDX6-foci-analysis>).

**Expanded View** for this article is available online.

### Acknowledgements

We thank D. H. Castrillon for kindly providing *Muh-Cre* mice. We also thank A. Suzuki for providing the DAZL antibody and A. Nakamura for critical reading of the manuscript. This work was supported by a Grant-in-Aid for Scientific Research to Y.K. (No. 17K07422) and Y.S. (No. 26251025) from JSPS, and by a Grant-in-Aid for Scientific Research on Innovative Areas from MEXT to Y.K. (No. 26114512, 16H01259, and 19H05247) and T.I. (No. 26114506).

### Author contributions

YK designed the experiments. YK, TI, JM, and MS performed the experiments and analyzed the results. TK performed RNA-sequencing and YN analyzed the sequence data. YK and YS generated knockout mice and wrote the manuscript. All authors commented on the results and agreed on the final manuscript.

### Conflict of interest

The authors declare that they have no conflict of interest.

### References

1. Pepling ME (2006) From primordial germ cell to primordial follicle: mammalian female germ cell development. *Genesis* 44: 622–632
2. Bowles J, Knight D, Smith C, Wilhelm D, Richman J, Mamiya S, Yashiro K, Chawengsaksophak K, Wilson MJ, Rossant J *et al* (2006) Retinoid signaling determines germ cell fate in mice. *Science* 312: 596–600
3. Koubova J, Menke DB, Zhou Q, Capel B, Griswold MD, Page DC (2006) Retinoic acid regulates sex-specific timing of meiotic initiation in mice. *Proc Natl Acad Sci USA* 103: 2474–2479
4. Pepling ME, Spradling AC (2001) Mouse ovarian germ cell cysts undergo programmed breakdown to form primordial follicles. *Dev Biol* 234: 339–351
5. Soyak SM, Amleh A, Dean J (2000) FIGalpha, a germ cell-specific transcription factor required for ovarian follicle formation. *Development* 127: 4645–4654
6. Trombly DJ, Woodruff TK, Mayo KE (2009) Suppression of Notch signaling in the neonatal mouse ovary decreases primordial follicle formation. *Endocrinology* 150: 1014–1024
7. Niu W, Wang Y, Wang Z, Xin Q, Wang Y, Feng L, Zhao L, Wen J, Zhang H, Wang C *et al* (2016) JNK signaling regulates E-cadherin junctions in germline cysts and determines primordial follicle formation in mice. *Development* 143: 1778–1787
8. Yan C, Wang P, DeMayo J, DeMayo FJ, Elvin JA, Carino C, Prasad SV, Skinner SS, Dunbar BS, Dube JL *et al* (2001) Synergistic roles of bone morphogenetic protein 15 and growth differentiation factor 9 in ovarian function. *Mol Endocrinol* 15: 854–866
9. Xu J, Gridley T (2013) Notch2 is required in somatic cells for breakdown of ovarian germ-cell nests and formation of primordial follicles. *BMC Biol* 11: 13
10. Morohaku K, Tanimoto R, Sasaki K, Kawahara-Miki R, Kono T, Hayashi K, Hirao Y, Obata Y (2016) Complete *in vitro* generation of fertile oocytes

- from mouse primordial germ cells. *Proc Natl Acad Sci USA* 113: 9021–9026
11. Hikabe O, Hamazaki N, Nagamatsu G, Obata Y, Hirao Y, Hamada N, Shimamoto S, Imamura T, Nakashima K, Saitou M *et al* (2016) Reconstitution *in vitro* of the entire cycle of the mouse female germ line. *Nature* 539: 299–303
  12. Lesch BJ, Page DC (2012) Genetics of germ cell development. *Nat Rev Genet* 13: 781–794
  13. Lin Y, Gill ME, Koubova J, Page DC (2008) Germ cell-intrinsic and -extrinsic factors govern meiotic initiation in mouse embryos. *Science* 322: 1685–1687
  14. Tay J, Richter JD (2001) Germ cell differentiation and synaptonemal complex formation are disrupted in CPEB knockout mice. *Dev Cell* 1: 201–213
  15. Medvedev S, Pan H, Schultz RM (2011) Absence of MSY2 in mouse oocytes perturbs oocyte growth and maturation, RNA stability, and the transcriptome. *Biol Reprod* 85: 575–583
  16. Mak W, Fang C, Holden T, Dratver MB, Lin H (2016) An important role of Pumilio 1 in regulating the development of the mammalian female germline. *Biol Reprod* 94: 134
  17. Racki WJ, Richter JD (2006) CPEB controls oocyte growth and follicle development in the mouse. *Development* 133: 4527–4537
  18. Guzeloglu-Kayisli O, Lalioti MD, Aydinler F, Sasson I, Ilbay O, Sakkas D, Lowther KM, Mehlmann LM, Seli E (2012) Embryonic poly(A)-binding protein (EPAB) is required for oocyte maturation and female fertility in mice. *Biochem J* 446: 47–58
  19. Gu W, Tekur S, Reinbold R, Eppig JJ, Choi YC, Zheng JZ, Murray MT, Hecht NB (1998) Mammalian male and female germ cells express a germ cell-specific Y-Box protein, MSY2. *Biol Reprod* 59: 1266–1274
  20. Yu J, Hecht NB, Schultz RM (2002) RNA-binding properties and translational repression *in vitro* by germ cell-specific MSY2 protein. *Biol Reprod* 67: 1093–1098
  21. Fukuda K, Masuda A, Naka T, Suzuki A, Kato Y, Saga Y (2018) Requirement of the 3'-UTR-dependent suppression of *Dazl* in oocytes for pre-implantation mouse development. *PLoS Genet* 14: e1007436
  22. Jain RG, Andrews LG, McGowan KM, Gao F, Keene JD, Pekala PP (1995) Hel-N1, an RNA-binding protein, is a ligand for an A + U rich region of the *GLUT1* 3' UTR. *Nucleic Acids Symp Ser* 209–211
  23. Jain RG, Andrews LG, McGowan KM, Pekala PH, Keene JD (1997) Ectopic expression of Hel-N1, an RNA-binding protein, increases glucose transporter (*GLUT1*) expression in 3T3-L1 adipocytes. *Mol Cell Biol* 17: 954–962
  24. Antic D, Lu N, Keene JD (1999) ELAV tumor antigen, Hel-N1, increases translation of neurofilament M mRNA and induces formation of neurites in human teratocarcinoma cells. *Genes Dev* 13: 449–461
  25. Decker CJ, Parker R (2012) P-bodies and stress granules: possible roles in the control of translation and mRNA degradation. *Cold Spring Harb Perspect Biol* 4: a012286
  26. Serman A, Le Roy F, Aigueperse C, Kress M, Dautry F, Weil D (2007) GW body disassembly triggered by siRNAs independently of their silencing activity. *Nucleic Acids Res* 35: 4715–4727
  27. Collier J, Parker R (2005) General translational repression by activators of mRNA decapping. *Cell* 122: 875–886
  28. Amano H, Itakura K, Maruyama M, Ichisaka T, Nakagawa M, Yamanaka S (2006) Identification and targeted disruption of the mouse gene encoding *ESG1* (PH34/ECAT2/DPPA5). *BMC Dev Biol* 6: 11
  29. Hinman MN, Lou H (2008) Diverse molecular functions of Hu proteins. *Cell Mol Life Sci* 65: 3168–3181
  30. Chalupnikova K, Solc P, Sulimenko V, Sedlacek R, Svoboda P (2014) An oocyte-specific ELAVL2 isoform is a translational repressor ablated from meiotically competent antral oocytes. *Cell Cycle* 13: 1187–1200
  31. Greenbaum MP, Iwamori N, Agno JE, Matzuk MM (2009) Mouse *TEX14* is required for embryonic germ cell intercellular bridges but not female fertility. *Biol Reprod* 80: 449–457
  32. Dong J, Albertini DF, Nishimori K, Kumar TR, Lu N, Matzuk MM (1996) Growth differentiation factor-9 is required during early ovarian folliculogenesis. *Nature* 383: 531–535
  33. Rankin T, Familiari M, Lee E, Ginsberg A, Dwyer N, Blanchette-Mackie J, Drago J, Westphal H, Dean J (1996) Mice homozygous for an insertional mutation in the *Zp3* gene lack a zona pellucida and are infertile. *Development* 122: 2903–2910
  34. Wu X, Viveiros MM, Eppig JJ, Bai Y, Fitzpatrick SL, Matzuk MM (2003) Zygote arrest 1 (*Zar1*) is a novel maternal-effect gene critical for the oocyte-to-embryo transition. *Nat Genet* 33: 187–191
  35. Rankin T, Talbot P, Lee E, Dean J (1999) Abnormal zonae pellucidae in mice lacking *ZP1* result in early embryonic loss. *Development* 126: 3847–3855
  36. Burns KH, Viveiros MM, Ren Y, Wang P, DeMayo FJ, Frail DE, Eppig JJ, Matzuk MM (2003) Roles of *NPM2* in chromatin and nucleolar organization in oocytes and embryos. *Science* 300: 633–636
  37. Rankin TL, O'Brien M, Lee E, Wigglesworth K, Eppig J, Dean J (2001) Defective zonae pellucidae in *Zp2*-null mice disrupt folliculogenesis, fertility and development. *Development* 128: 1119–1126
  38. Rajkovic A, Pangas SA, Ballow D, Suzumori N, Matzuk MM (2004) *NOBOX* deficiency disrupts early folliculogenesis and oocyte-specific gene expression. *Science* 305: 1157–1159
  39. Alberti S, Gladfelter A, Mittag T (2019) Considerations and challenges in studying liquid-liquid phase separation and biomolecular condensates. *Cell* 176: 419–434
  40. Ramaswami M, Taylor JP, Parker R (2013) Altered ribostasis: RNA-protein granules in degenerative disorders. *Cell* 154: 727–736
  41. Franzmann TM, Jahnel M, Pozniakovskiy A, Mahamid J, Holehouse AS, Nuske E, Richter D, Baumeister W, Grill SW, Pappu RV *et al* (2018) Phase separation of a yeast prion protein promotes cellular fitness. *Science* 359: eaao5654
  42. Voronina E, Seydoux G, Sassone-Corsi P, Nagamori I (2011) RNA granules in germ cells. *Cold Spring Harb Perspect Biol* 3: a002774
  43. Wilczynska A, Aigueperse C, Kress M, Dautry F, Weil D (2005) The translational regulator *CPEB1* provides a link between *dcp1* bodies and stress granules. *J Cell Sci* 118: 981–992
  44. Cougot N, Babajko S, Seraphin B (2004) Cytoplasmic foci are sites of mRNA decay in human cells. *J Cell Biol* 165: 31–40
  45. Sheth U, Parker R (2003) Decapping and decay of messenger RNA occur in cytoplasmic processing bodies. *Science* 300: 805–808
  46. Sen GL, Blau HM (2005) Argonaute 2/RISC resides in sites of mammalian mRNA decay known as cytoplasmic bodies. *Nat Cell Biol* 7: 633–636
  47. Liu J, Valencia-Sanchez MA, Hannon GJ, Parker R (2005) MicroRNA-dependent localization of targeted mRNAs to mammalian P-bodies. *Nat Cell Biol* 7: 719–723
  48. Kedersha NL, Gupta M, Li W, Miller I, Anderson P (1999) RNA-binding proteins TIA-1 and TIAR link the phosphorylation of eIF-2 alpha to the assembly of mammalian stress granules. *J Cell Biol* 147: 1431–1442
  49. Inoue M, Muto Y, Sakamoto H, Yokoyama S (2000) NMR studies on functional structures of the AU-rich element-binding domains of Hu antigen C. *Nucleic Acids Res* 28: 1743–1750

50. Gallardo T, Shirley L, John GB, Castrillon DH (2007) Generation of a germ cell-specific mouse transgenic Cre line, Vasa-Cre. *Genesis* 45: 413–417
51. Reddy P, Liu L, Adhikari D, Jagarlamudi K, Rajareddy S, Shen Y, Du C, Tang W, Hamalainen T, Peng SL et al (2008) Oocyte-specific deletion of Pten causes premature activation of the primordial follicle pool. *Science* 319: 611–613
52. John GB, Gallardo TD, Shirley LJ, Castrillon DH (2008) Foxo3 is a PI3K-dependent molecular switch controlling the initiation of oocyte growth. *Dev Biol* 321: 197–204
53. Keene JD (2007) RNA regulons: coordination of post-transcriptional events. *Nat Rev Genet* 8: 533–543
54. Fukao A, Sasano Y, Imataka H, Inoue K, Sakamoto H, Sonenberg N, Thoma C, Fujiwara T (2009) The ELAV protein HuD stimulates cap-dependent translation in a Poly(A)- and eIF4A-dependent manner. *Mol Cell* 36: 1007–1017
55. Lei L, Spradling AC (2016) Mouse oocytes differentiate through organelle enrichment from sister cyst germ cells. *Science* 352: 95–99
56. Takahara T, Maeda T (2012) Transient sequestration of TORC1 into stress granules during heat stress. *Mol Cell* 47: 242–252
57. Thedieck K, Holzwarth B, Prentzell MT, Boehlke C, Klasener K, Ruf S, Sonntag AG, Maerz L, Grellescheid SN, Kremmer E et al (2013) Inhibition of mTORC1 by astrin and stress granules prevents apoptosis in cancer cells. *Cell* 154: 859–874
58. Wippich F, Bodenmiller B, Trajkovska MG, Wanka S, Aebersold R, Pelkmans L (2013) Dual specificity kinase DYRK3 couples stress granule condensation/dissolution to mTORC1 signaling. *Cell* 152: 791–805
59. Nakamura A, Amikura R, Hanyu K, Kobayashi S (2001) Me31B silences translation of oocyte-localizing RNAs through the formation of cytoplasmic RNP complex during *Drosophila* oogenesis. *Development* 128: 3233–3242
60. Navarro RE, Shim EY, Kohara Y, Singson A, Blackwell TK (2001) cgh-1, a conserved predicted RNA helicase required for gametogenesis and protection from physiological germline apoptosis in *C. elegans*. *Development* 128: 3221–3232
61. Saatcioglu HD, Cuevas I, Castrillon DH (2016) Control of oocyte reawakening by kit. *PLoS Genet* 12: e1006215
62. Shimamoto S, Nishimura Y, Nagamatsu G, Hamada N, Kita H, Hikabe O, Hamazaki N, Hayashi K (2019) Hypoxia induces the dormant state in oocytes through expression of Foxo3. *Proc Natl Acad Sci USA* 116: 12321–12326
63. Nagamatsu G, Shimamoto S, Hamazaki N, Nishimura Y, Hayashi K (2019) Mechanical stress accompanied with nuclear rotation is involved in the dormant state of mouse oocytes. *Sci Adv* 5: eaav9960
64. Sakai K, Miyazaki J (1997) A transgenic mouse line that retains Cre recombinase activity in mature oocytes irrespective of the cre transgene transmission. *Biochem Biophys Res Commun* 237: 318–324
65. Farley FW, Soriano P, Steffen LS, Dymecki SM (2000) Widespread recombinase expression using FLP<sub>er</sub> (flipper) mice. *Genesis* 28: 106–110
66. Pedersen T, Peters H (1968) Proposal for a classification of oocytes and follicles in the mouse ovary. *J Reprod Fertil* 17: 555–557
67. Pau G, Fuchs F, Sklyar O, Boutros M, Huber W (2010) EBImage—an R package for image processing with applications to cellular phenotypes. *Bioinformatics* 26: 979–981
68. Kim D, Pertea G, Trapnell C, Pimentel H, Kelley R, Salzberg SL (2013) TopHat2: accurate alignment of transcriptomes in the presence of insertions, deletions and gene fusions. *Genome Biol* 14: R36
69. Zhang Y, Liu T, Meyer CA, Eeckhoute J, Johnson DS, Bernstein BE, Nusbaum C, Myers RM, Brown M, Li W et al (2008) Model-based analysis of ChIP-Seq (MACS). *Genome Biol* 9: R137
70. Zhu LJ, Gazin C, Lawson ND, Pages H, Lin SM, Lapointe DS, Green MR (2010) ChIPpeakAnno: a Bioconductor package to annotate ChIP-seq and ChIP-chip data. *BMC Bioinformatics* 11: 237
71. Durinck S, Spellman PT, Birney E, Huber W (2009) Mapping identifiers for the integration of genomic datasets with the R/Bioconductor package biomaRt. *Nat Protoc* 4: 1184–1191